Characterization and metrology of nanoclusters-based nanostructures

Philippe Pareige, Manuel Roussel, Lardé Rodrigue, Ramesh Pratibha Nalini, Fabrice Gourbilleau, Etienne Talbot

▶ **To cite this version:**

Philippe Pareige, Manuel Roussel, Lardé Rodrigue, Ramesh Pratibha Nalini, Fabrice Gourbilleau, et al.. Characterization and metrology of nanoclusters-based nanostructures. ECS Transactions, 2011, 35 (18), pp.55. 10.1149/1.3647904 . hal-01633471

HAL Id: hal-01633471
https://hal.science/hal-01633471v1

Submitted on 27 Jan 2023

HAL is a multi-disciplinary open access archive for the deposit and dissemination of scientific research documents, whether they are published or not. The documents may come from teaching and research institutions in France or abroad, or from public or private research centers.

L'archive ouverte pluridisciplinaire **HAL**, est destinée au dépôt et à la diffusion de documents scientifiques de niveau recherche, publiés ou non, émanant des établissements d'enseignement et de recherche français ou étrangers, des laboratoires publics ou privés.

Characterization And Metrology Of Nanoclusters-Based Nanostructures

P. Pareige[a], M. Roussel[a], R. Lardé[a], R. Pratibha-Nalini[b], F. Gourbilleau[b], and E. Talbot[a]

[a] Groupe de Physique des Matériaux (GPM), Université et INSA de Rouen, UMR CNRS 6634, Avenue de l'Université, BP 12, 76801 Saint Etienne du Rouvray, France
[b] Centre de Recherche sur les Ions, les Matériaux et la Photonique (CIMAP), CEA/CNRS/ENSICAEN/UCBN, 6 Bd. Maréchal Juin, 14050 Caen Cedex 4, France

Silicon nanoclusters have attracted much interest during the past few years due to their optical and electrical properties (light emission, carrier storage…). These properties are strongly dependent on structural characteristics of nanoclusters (Si-nanoclusters size, distribution, surrounding matrix composition, interface nature…). Thus it is essential to provide characterization procedures which fully describe such systems. Unfortunately, conventional analysis methods such as HRTEM, EFTEM or X-ray diffraction often encounter severe difficulties to measure these parameters. In the present study, Atom Probe Tomography (APT) has been used to investigate structural properties of silicon nanoclusters embedded in silica. We studied SiO_x/SiO_2 MLs which are composed of 4 nm thick SiO_x layers and 4nm thick SiO_2 layers containing Si-ncs. Bulk silicon dioxide doped with Erbium and containing Si-ncs dedicated to light amplification has also been studied. We compare data provided by HRTEM, APT and previous studies found in the literature.

Introduction

Silicon nanoclusters (Si-ncs) embedded in a dielectric matrix are known to exhibit light emission properties **[1]** and charge trapping possibilities **[2]**. Therefore, the possibility of optoelectronic and microelectronic devices containing Si-ncs has been deeply studied during the past few years **[2-4]**. As an example, in photovoltaic cells, Si-ncs permits to absorb a larger range of solar emission spectrum than bulk silicon, increasing photovoltaic cells efficiency **[5]**. In planar waveguide amplifier, a device combining Er^{3+} ions and Si-ncs in a silica matrix lead to new generations of light sources at the standard telecommunication wavelength of 1.54 µm **[6,7]**. Using Si-ncs instead of poly-silicon in transistor floating gates allow better performances for new generations of non-volatile memories **[2]**.

For each one of these applications, structural properties of Si-ncs and their surrounding matrix are key parameters. Size distribution of Si-ncs directly controls the band gap of the system and thus allows a tunable photoluminescence (PL) of Si-ncs **[5, 7-10]**. Defects in the matrix and at Si-ncs interface are known to play an important role in photonic emission too. Si-ncs distribution in the dielectric is determining concerning light amplification in waveguides **[3, 4]** and for writing-erasing speed in non-volatile

memories **[11]**. Surrounding dielectric composition is also of prime interest because it influence directly charge retention and photonic emission.

These structural properties are strongly dependent on the elaboration process which usually consists in two steps. Firstly, silicon rich silicon oxide is prepared by deposition techniques (CVD **[12]**, magnetron sputtering **[13],** …) or by ionic implantation of silicon in silica **[10]**. In the second time, annealing treatment is performed in order to induce the phase separation between Si and SiO_2 **[13-15]**. The control of Si-ncs size is commonly achieved by preparing SiO_x/SiO_2 multilayers (MLs). During the phase separation process, SiO_2 layers act as diffusion barrier for silicon atoms and limit the Si-ncs growth.

Many structural studies have been focused on the characterization of such systems using conventional techniques (HRTEM, EFTEM, defocused bright field, EELS, SIMS, XRD **[16-23]**) in order to provide information about the matrix composition, Si-ncs size, interface between clusters and matrix or Si-ncs distribution. However a multi technique approach is essential to provide accurate information. In this study we show complementary information that can be provided by atom probe tomography (APT). The present paper discusses two kind of sample: SiO_X/SiO_2 multilayers and thin layer of Er-doped silicon rich silicon oxide.

Experimental

Elaboration

Silicon rich silicon oxide layers were elaborated on p-type [100]-oriented Si wafers by reactive magnetron sputtering.

In the case of SiO_X/SiO_2 MLs, pure SiO_2 targets are sputtered. Alternation between pure Ar plasma and mixed H_2-Ar (50-50) plasma permits to deposit a sequence of pure SiO_2 layers and SiO_X layers. The MLs were grown at 650°C with a power density of 1.3 $W.cm^{-2}$. Deposition time permits to tune the thickness of each layer, which have been measured after the deposition process by HRTEM imaging and have been estimated to be 4 nm for each layer (SiO_2 and SiO_X). This deposition process was described in detail by Ternon *et al.* **[15]**. Annealing treatment has been realized after the deposition during 1 h at 900°C under N2. These conditions have already shown their efficiency to promote phase separation in these systems.

Er doped silicon rich silicon oxide thin films were obtained by co-sputtering of Er_2O_3 and SiO_2 targets in pure argon plasma on substrate kept at 500 °C. The Er content and the Si excess were independently monitored through the control of the RF power applied on corresponding cathode. More details on the fabrication processes can be found in reference **[23, 24]**. 200 nm thick layers were deposited on p-type [100]-oriented Si wafers. An annealing treatment of 1h at 1100°C has been performed in order to induce the precipitation of Si-ncs.

Atom Probe Tomography

APT analyses are carried out on laser assisted wide angle tomographic atom probe (LA-WATAP - CAMECA model). APT is an atomic resolution 3D chemical microscope.

Its principle relies on the field evaporation of atoms from the surface of the analyzed specimen and their chemical identification by time-of-flight mass spectrometry **[25, 26]**. The specimen has to be prepared in the shape of a sharp tip (less than 50 nm of curvature radius). This tip is then submitted to a high positive voltage (3-15kV) under high vacuum (10^{-13} Bar) and low temperature conditions (80°K). The high voltage applied to such a sharp specimen induces a high electric field at the apex of the tip (several hundred $V.nm^{-1}$). Surface ions are ionized and evaporated by the mean of UV (343 nm) femtosecond laser pulses (50 nJ, 350 fs, 100 kHz). Once evaporated, ions are accelerated toward a position-sensitive detector. The time of flight of each evaporated ion is measured between the laser pulse and the impact on the detector. Knowing the time of flight and the flying distance permits to calculate the mass-to-charge ratio and deduce the chemical nature of each ion. The use of geometrical assumptions and the knowledge of impact position on the detector permit the calculation of the position of the atom before its evaporation. By combining these chemical information and spatial information, APT provides a 3D reconstruction of the sample at the atomic scale.

Sample preparation

As mentioned above, samples have to be tip-shaped with a curvature radius smaller than 50 nm. The sample preparation, which is an essential part for APT analyses, is described on fig.1. A Ga focused ion beam (FIB) coupled with a scanning electron microscope (SEM), a gas injection system and a micromanipulator are used to prepare samples. In order to prevent Ga implantation and sample degradation, a sacrificial platinum layer (approximately 400nm) is deposited on the top of the sample. A thin lamella is prepared from deposited layer using successive milling steps (figure 1.a). This lamella is extracted from the bulk material with a micromanipulator and welded with platinum on top of stainless steel needles (as shown in figure 1.b). Stainless steel needles mounted with sample posts (figure 1.c) are sharpened using successive concentric annular milling (figures 1.d). The final sharpening step is carried out at low accelerating voltage (2kV), in order to prevent Ga implantation in the sample. This whole procedure has already been reported to ensure Ga-free tips **[27]**.

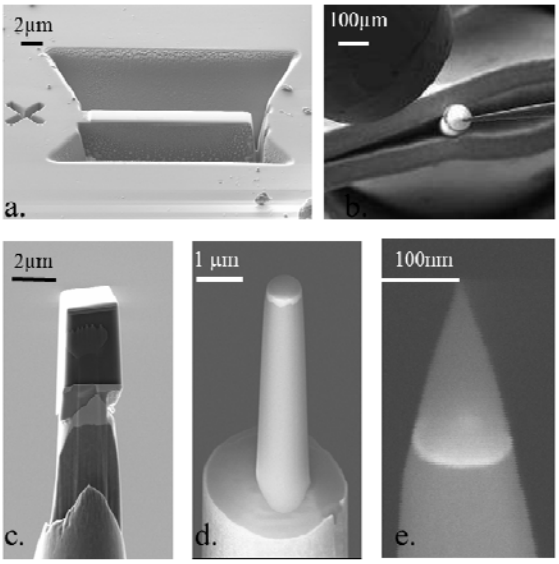

Figure 1. FIB-SEM procedure for APT sample preparation. a. Extraction of a lamella using the Lift-out method. b. The lamella is welded onto a steel needle (platinum weld). c. A post is extracted from the lamella. d. and e. Successive annular milling steps permit to obtain a very sharp tip which curvature radius does not exceed 50nm.

Results and discussion

SiO_X/SiO_2 multilayers

SiO_x/SiO_2 MLs have been studied successively by HRTEM and APT. These analyses are reported in figure 2. HRTEM image is reported in figure 2.a. This cross-section micrography permits to evidence two crystallized Si-ncs (highlighted with red circles) in SiO_x/SiO_2 stacking sequence (highlighted with white lines). Nevertheless, HRTEM allows to image only Si-ncs which fulfilled diffraction conditions. 3D chemical map provided by APT is reported in figure 2.b. On this map, each dot represents a single atom. A cluster identification algorithm permits to identify Si atoms belonging to any Si-ncs. For the sake of clarity only silicon atoms belonging to Si-ncs and oxygen atoms are represented on this map **[28, 29]**.

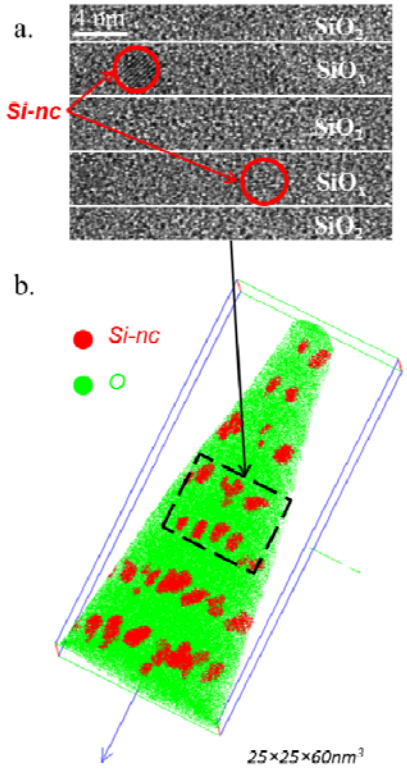

Figure 2. a. HRTEM micrography of SiO_2/SiO_x multilayers in cross-sectional view. Red circles highlight crystallized Si-ncs. b. 3D reconstruction of SiO_2/SiO_x MLs provided by APT analysis. Cluster identification algorithm permits to identify Si atoms belonging to Si-ncs (red dots). Each green dot corresponds to an oxygen atom.

It is of prime interest to determine the structure of particles which control the optical properties. As for the density of particle and their location, it determines the number of charges that can be trapped and writing-erasing speed in microelectronic devices. Both techniques clearly evidence Si-ncs in silicon oxide. HRTEM experiments permit to

evidence Si-ncs which are crystallized surrounded by an amorphous matrix. HRTEM also permits to observe the morphology of Si-ncs which appears to be spherical. Unfortunately amorphous clusters are not visible as well as clusters which are not in diffraction conditions. In the same way, APT is able to chemically identify all the Si-ncs (crystallize and amorphous) but is unable to distinguish their crystalline structure. This is the reason why more clusters are observed in APT. Thus a better estimation of the number density of particle is achievable using atom probe rather than conventional electron microscopy. This APT value is estimated to $10\times10^{18} \pm 1\times10^{18}$Si-ncs.cm^{-3}. Other studies show that Energy Filtered - TEM is able to evidence amorphous clusters **[18-20]**. However, identification of Si phase relies on the deconvolution of Si peak on EELS spectra **[19]**. Besides it gives only access to planar projection of three dimensional objects. These considerations lead to great uncertainty concerning the measurement of number density of particles.

Measuring the size of Si-ncs is imperative in Si-nc based materials because the Si-ncs size directly determines the band gap energy of the system. HRTEM allow to measure approximately the size of Si-ncs which appears to be around 3-4nm. However it is important to understand that this measurement does not take into account amorphous clusters. EFTEM has been demonstrated to be more accurate to estimate a size distribution of Si-ncs **[18-20]**. Nevertheless Si-nc size strongly depends on data treatment and contrast enhancement. Additionally small clusters (smaller than 1nm) cannot be detected. Thus the measurement of the size distribution by electron microscopy can be difficult. XRD has also been used to measure the mean radius of Si-ncs but it appears that the lack of Si-ncs in volume leads to great uncertainty **[22]**. By using APT data it becomes very easy to measure the size of any Si-nc. Assuming that Si-ncs are spherical, a diameter can be calculated by counting the number of Si atoms within a Si-nc. This procedure has been used in previous papers and is able to provide a very accurate size distribution of particles and a mean diameter **[28]**. Each size measurement is accurate up to 0.1 nm. In addition, this measurement is not submitted to interface uncertainty as it can be observed in the case of EFTEM imaging where the size distribution strongly depends on the image treatment. The interface of Si-ncs has been clearly evidence as a SiO_2 shell in a previous paper and is not taken into account in the size measurement. As shown in figure 3, the size of the precipitates varies from 0.5 to 4.5 nm. The mean cluster diameter is 2.9 nm. More than 50% of the particle sizes lie in the range of 3-4 nm which corresponds to the size of the SiO_x sublayer (4nm).

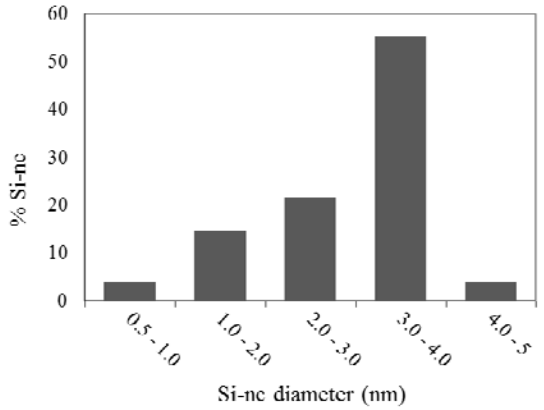

Figure 3. Si-ncs size distribution in SiO_x/SiO_2 MLs annealed 1h at 900°C

As mentioned above the quality of the oxide surrounding Si-ncs plays an important role concerning the photonic emission and the charge retention. It is essential to measure accurately this composition. However HRTEM cannot provide such information. The only study which deals with phase composition is reported by Spinela et al. In this study phase compositions are extrapolated from EELS spectra **[19]**. However, composition can only be determined under given assumptions like monodisperse Si-ncs. Thanks to its ability to determine local composition at the atomic scale, APT appears to be a powerful tool concerning this question. Indeed it becomes possible to measure matrix composition by avoiding Si-ncs. Doing this in the sample annealed 1h at 900°C permits to measure a composition of of 41.9 ± 0.3 at.% of Si. This value, significantly higher than the value in pure silica, evidences an incomplete phase separation for this annealing treatment. Such a non-stoichiometric oxide can be detrimental for optical and electrical properties of the MLs and can hardly be highlighted with other techniques.

Er doped silicon rich silica

In another type of photonic device, Er doped silicon rich silica (Er-SiO_x), functional properties are strongly dependant of the Si-ncs growth and Er^{3+} ions location in the silica matrix with specific regard to the distance between Er atoms and Si-ncs. We have studied a 200 nm thick layer of silicon rich silica doped with high content Er^{3+} ions (~$1.0x10^{21}$ $at.cm^{-3}$). This sample has been annealed for 1h at 1100°C under N_2 atmosphere. In this paper, we have investigated the distribution of Er ions and Si-nc growth for the as-deposited and annealed sample to overcome the limited quantitative information obtain with conventional techniques of structural characterization and to answer to critical issue of the optimized microstructure leading to achieve a net gain in such system.

Figure 4 shows the 3D reconstruction of the as-deposited Er-doped SiO_x sample after an APT experiment. This results evidence a homogenous mapping of the three chemical elements in the as-deposited sample. Statistical data treatments have been performed to confirm this results and suggesting that no silicon or erbium clustering occurs during the elaboration process. The composition of the sample has been estimated to be X_{Si}=35.1±0.4 at.%, X_O=63.2±0.4 at.% and X_{Er}=1.7±0.4 at.%.

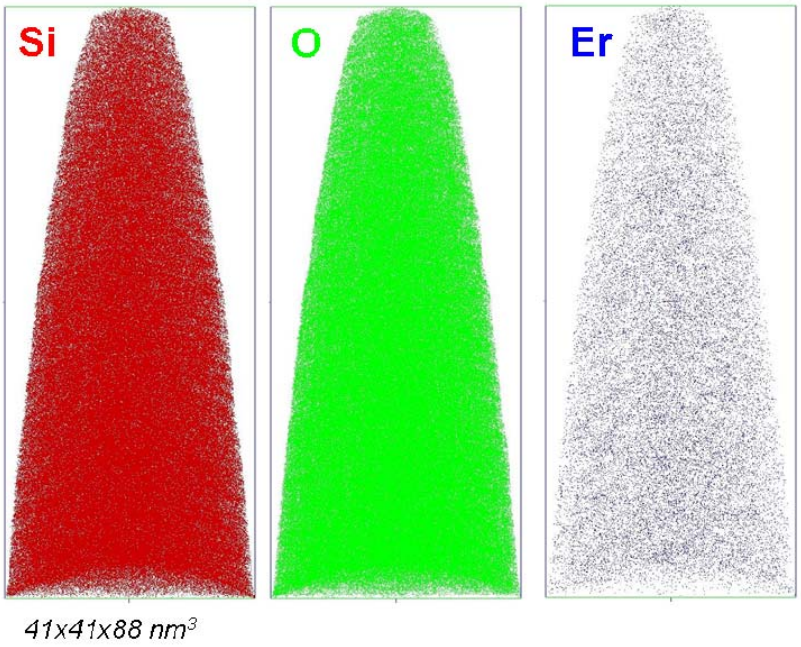

Figure 4: 3D reconstruction of Er-doped silicon rich silica in the as-deposited state. Silicon (red), Oxygen (green) and Erbium (blue) atoms are represented. The volume is 41x41x88 nm^3.

Figure 5 shows the 3D distribution of the chemical species in the Er-doped sample annealed at 1100°C during 1h. For clarity reasons, only Si and Er atoms which belong to clusters are represented.

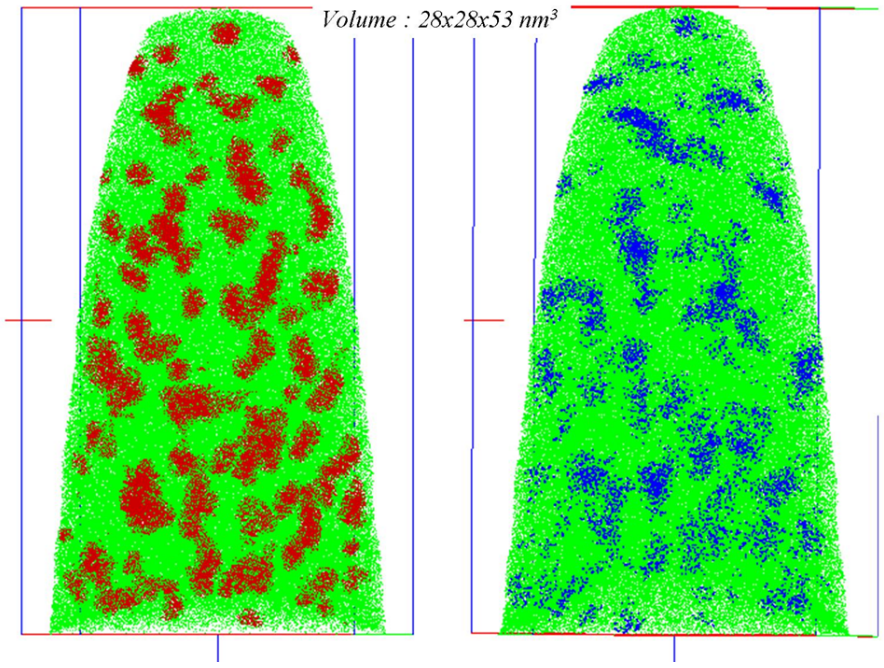

Figure 5: 3D reconstruction of Er-doped silicon rich silica after 1h annealing at 1100°C. Silicon (red), Oxygen (green) and Erbium (blue) atoms are represented. The volume is 28x28x53 nm^3.

As it is clearly revealed, Si nanoclusters are present in the volume due to the phase separation which occurs between Si and SiO_2 during the annealing. Si-ncs are homogeneously distributed in the volume with a density of $3.1 \pm 0.2 \times 10^{18}$ Si-ncs.cm^{-3}. In the same time, Er-rich clusters (Er-ncs) have also been evidenced with a large density (~2.0×10^{18} Er-ncs.cm^{-3}). No particular morphology has been extracted from the Er-ncs which appears to be isolated and homogenously distributed. This result demonstrates that the annealing step leads to the decomposition of the initial homogeneous SiOEr layers in a complex system composed of three phases: silica matrix, pure Si nanoclusters and Er-rich particles. As a consequence of segregation of Er atoms during annealing, they cannot give a contribution to the emission properties of the sample. This explains why the increase of Er concentration in such a system cannot improve the gain of Er-doped devices.

Conclusion

Atom probe tomography has been used to investigate the microstructure of Si-nanoclusters based devices. APT ability of providing 3D maps at the atomic scale is of great interest in such systems. We highlighted the possibility of measuring Si-nc size size and distribution, Si-nc density and matrix composition in SiO_x/SiO_2 ML systems. We evidenced that an annealing treatment of 1h at 900°C in SiO_x containing 50% of Si is unable to complete phase separation. In Er-SiO_x systems we studied spatial distribution of Si-ncs and Er dopants in 3D. We also evidence the formation of both Si-ncs and Er-ncs.

Acknowledgments

This study was supported by the upper Normandy Research and the French Ministry of Research in the framework of Research Networks of Upper-Normandy. The authors also acknowledge “Le Fond Européen de Développement Régional” (FEDER) for his support.

References

1. L. Canham, *Appl. Phys. Lett.* **57**, 1046 (1990).
2. S. Tiwari, F. Rana, H. Hanafi,A. Harstein, E. Crabbe,K. Chan, *Appl. Phys. Lett.* **68**, 1377 (1996).
3. A. T. Fiori, N. Ravindra, *J. Electron. Mater.*, **32**, 1043 (2003)
4. S. Oda, S. Huang, M. A. Salem, D. Hippo, H. Mizuta, *Physica E*, **38**, 59 (2007).
5. F. Gourbilleau, C. Ternon, D. Maestre, O. Palais, C. Dufour, *J. Appl. Phys*, **106**, 013501 (2009)
6. M. Fujii, M. Yoshida, Y. Kanzawa, S. Hayashi, K. Yamamoto, *Appl. Phys. Lett*. **71**, 1198 (1997)

7. D. Pacifici, G. Franzo, F. Priolo, F. Iacona, L. Dal Negro, *Phys. Rev. B*, **67**, 245301 (2003)
8. N. Hill, K. Whaley, *Phys. Rev. Lett*.,**75**, 1130 (1995)
9. T. Creazzo, B. Redding, E. Marchena, J. Murakowski, D. Prather, *J Luminescence*, **130**, 631 (2010)
10. A. Hryciw, A. Meldrum, K. Buchanan, C. White, Nucl. Instrum. Methods. *Phys. Res. B*, **222**, 469 (2004)
11. S. Schamma, C. Bonafosa, H. Coffina, N. Cherkashina, M. Carradaa, G. Ben Assayaga, A. Claveriea, M. Tencéb and C. Colliexb, *Ultramicroscopy*, **108-4**, 346 (2008)
12. Y. Kanemitsu, *Phys Rev B*, **53**, 13515 (1996)
13. F. Gourbilleau, X. Portier, C. Ternon, P. Voivenel, R. Madelon, R. Rizk, *Appl. Phys. Lett*., **78**, 3058 (2001)
14. T. Baron, F. Mazen, C. Busseret, A. Souifi, P. Mur, F. Fournel, M. Séméria, H. Moriceau, B. Aspard, P. Gentile, N. Magnea, *Microelectron. Eng.*, **61**, 511 (2002)
15. C. Ternon, F. Gourbilleau, X. Portier, P. Voidevel, C. Dufour, *Thin Solid Films*, **419**, 5 (2002)
16. F. Iacona, G. Franzo, C. Spinella, *J. Appl. Phys.*, **87,** 1295 (2000)
17. S. Boninelli, F. Iacona, C. Bongiorno, C. Spinella, F. Priolo, *Mater. Res. Soc. Proc*. **817**, L6.12.1 (2004)
18. S. Schamm, C. Bonafos, H. Coffin, N. Cherkashin, M. Carrada, G. Ben Assayag, A. Claverie, M. Tencé, C. Colliex, *Ultramicroscopy*, **108**, 346 (2008)
19. C. Spinella, G. Nicotra, C. Bongiorno, E. Rimini, *Appl. Phys. Lett.,* **87**, 044102 (2005)
20. J. Wang, X. Wang, Q. Li , A. Hryciw, A. Meldrum, *Philos Mag*, **87**, 11 (2010)
21. A. Yurtsever, M. Weyland, D. Muller, *Appl. Phys. Lett*., **89**, 151920 (2006)
22. D. Comedi, O. H. Y. Zalloum, E. A. Irving, J. Wojcik, T. Roschuk, M. J. Flynn, P. Mascher, *J. Appl. Phys*., **99**, 023518 (2006)
23. F. Gourbilleau, M. Levalois, C. Dufour, J. Vicens, R. Rizk, *J. Appl. Phys.*, **95**, 3717 (2004)
24. K. Hijazi, L. Khomenkova, F. Gourbilleau, J. Cardin, R. Rizk, *J. Lumin.*, **129**, 1886 (2009)
25. E. Muller, J. Panitz, S. McLane. *Rev. Sci. Instrum.*, **39**, 83 (1968)
26. B. Gault, F. Vurpillot, A. Vella, M. Gilbert, A. Menand, D. Blavette, B. Deconihout, *Rev. Sci. Instrum*., **77**, 043705 (2006)
27. K. Thompson, D. Lawrence, D. J. Larson, J. D. Olson, T. F. Kelly, B. Gorman, *Ultramicroscopy*, **107**, 131 (2007)
28. E. Talbot, R. Lardé, F. Gourbilleau, C. Dufour, P. Pareige, *Eur. Phys. Lett*., **87**, 26004 (2009)
29. M. Roussel, E. Talbot, F. Gourbilleau, P. Pareige, *Nanoscale Res. Lett*., **6**, 164 (2011)